Hydraulic Tomography: 3-D Hydraulic Conductivity and Fracture Network Connectivity in a Contaminated Mudstone Aquifer

Warren Barrash (wbarrash@boisestate.edu) (Boise State University, Boise, ID)
Claire R. Tiedeman (U.S. Geological Survey, Menlo Park, CA)
Colby Thrash (Decagon Instruments, Pullman, WA)
Jeremy Patterson (University of Wisconsin-Madison, WI)
Carole Johnson (U.S. Geological Survey, Storrs, CT)

INTRODUCTION

Effective in situ remediation of source zones in fractured-rock aquifers requires high-resolution characterization of the extreme heterogeneity of fracture network geometry and of hydraulic conductivity (K) within and between fractures. This characterization is needed for accurate flow and transport modeling to support effective, and even "surgical," in situ remediation (Leeson et al., 2013; NAS, 2015). In this study we adapt hydraulic tomography (HT) field and modeling methods to estimate the actual three-dimensional (3-D) distributions of K, the fracture network, and fracture connectivity in an aquifer volume of investigation to the extent possible. HT field testing was conducted in the DNAPL-contaminated mudstone aquifer at the former Naval Air Warfare Center (NAWC) in the Newark Basin near Trenton, New Jersey, USA (Figure 1). In this paper we give brief overviews of the HT method and field site, then present examples of (a) field results from HT tests showing complexity of the fractured system, (b) 3-D K results from HT modeling to locate important hydrogeological features, and (c) drawdown simulations to locate connectivity in the 3D fracture network and explain the complex drawdown behavior seen in the field results. Because it is difficult to adequately describe 3-D K structure and hydraulic behavior in words, we rely heavily on figures and captions to provide examples of drawdown following different paths (connectivity) in the 3-D fracture network to reach different observation zones.

HYDRAULIC TOMOGRAPHY METHOD AND FIELD TESTING

HT is a 3-D subsurface "imaging" method whereby: (a) a volume of aquifer is investigated with a series of pumping tests, each test from a different individual packer-isolated well interval, with drawdowns continuously monitored in a dense array of other packer-isolated intervals, and (b) the 3-D K distribution for the volume is estimated ("imaged") with inverse modeling using drawdown responses from all the pumping tests together. The 3-D HT approach used here is an adaptation to a fractured rock aquifer of the method used in two unconsolidated sedimentary aquifers by Cardiff et al. (2013) and Hochstetler et al. (2016). For HT testing at NAWC, we inverted data from 42 tests conducted in 2015 and 2016 from packer-isolated intervals in seven wells of a research wellfield (wells 83BR – 89BR in Figure 1B; often referred to by their numbers (83-89) in this paper). We monitored 30 to 38 observation intervals per test. MODFLOW was used for the flow modeling. To avoid biasing the inversion solution, we did not use prior assumptions about fracture locations or statistical models of fracture sets. We used a fixed spatially uniform specific storage ($Ss=5\times10^{-6}$ m^{-1}) that is consistent with NAWC site literature (Tiedeman et al., 2010). Five additional tests are reserved for validation; other evaluation measures have included calibration curve matches and statistics, K uncertainty, and comparison with geophysical logs and rock core, but are not discussed here. Work in progress is investigating possible improvements in K-field accuracy and resolution with refined discretization of the parameter estimation grid and with estimation of the 3-D Ss distribution.

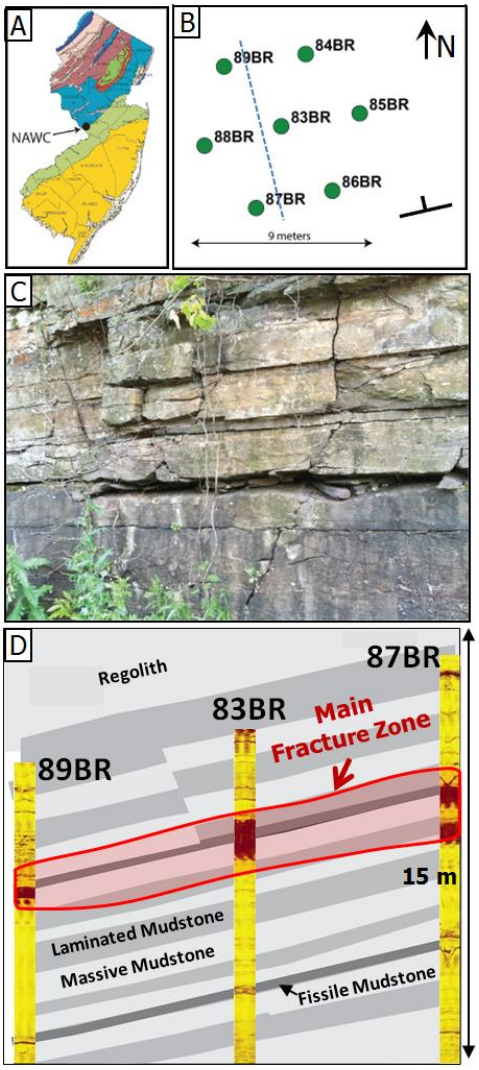

Figure 1. Former Naval Air Warfare Center (NAWC) field site for HT testing. A. NAWC is near Trenton, NJ and is underlain by fractured sedimentary rocks of the Lockatong Formation (Fm) within the Newark Basin (Lacombe and Burton, 2010). **B.** Plan view of wellfield used for HT testing. Dashed line shows cross-section in D. **C.** Outcrop of Lockatong Fm mudstones near NAWC. **D.** Cross section through wellfield showing generalized lithology and acoustic televiewer (ATV) logs. Beds dip 20-25°. Bedding plane fractures that dominate flow occur mostly in fissile mudstones and vary in K laterally. Bedding plane fractures in laminated and massive mudstones, and high-angle connecting fractures, generally are lower K and vary in density of occurrence and connectivity. A highly fractured fissile mudstone and hydraulically connected fractures in adjacent mudstones (i.e., dark maroon bands in the, ATV logs) form a Main Fracture Zone (MFZ) that includes regions of very-high K (Tiedeman et al., 2010; Robinson et al., 2015).

FIELD RESULTS: 3D K HETEROGENEITY

Log-log drawdown versus time curves show behavior indicative of heterogeneity within and between fractures, including: for a given test, curves for different intervals of a given observation well cross one another; for tests conducted in different wells but in similar stratigraphic units, curves for a given observation interval can show similar responses or can have highly variable shapes, orders, and magnitude of time-lag and/or drawdown. Figure 2 illustrates some of these behaviors that can be interpreted as heterogeneity within the MFZ (Figure 2B) and between fractures (Figure 2D).

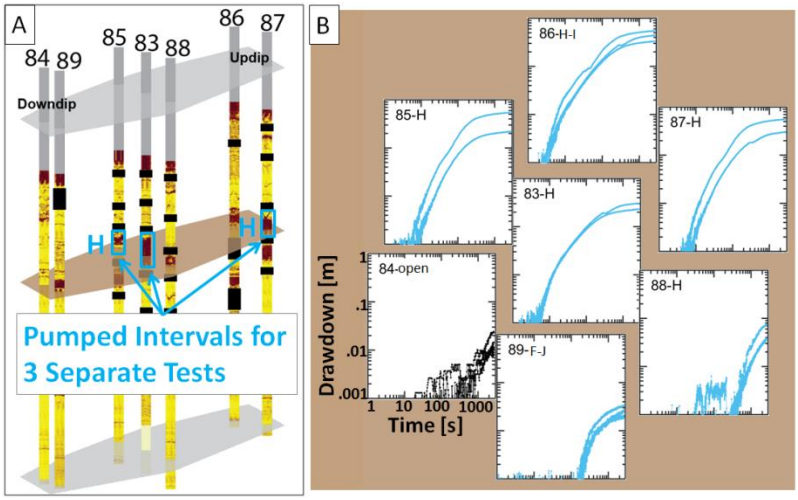

Figure 2. Drawdown data from tests at interval H in wells 83, 85, and 87 provide examples of heterogeneity within MFZ bedding plane fractures and of complex connectivity in vertical dimension. **A.** 3-D perspective diagram of wellfield with ATV logs, packed-off pumping and observation intervals, and

brown plane representing dip of the

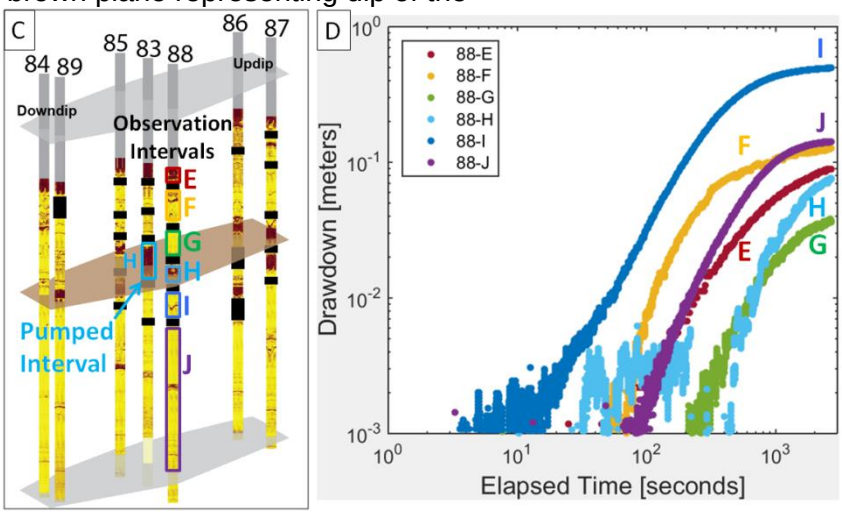

MFZ. **B.** Log-log drawdown versus time curves for observation intervals open to the MFZ for three tests with pumping from the MFZ (in wells 83, 85, and 87) show consistent results overall for the tests but also show significant lateral heterogeneity with two different types of behaviors: (1) rapid response and large drawdown in 83, 85, 86, and 87 (drawdown in pumped intervals not shown); (2) slower response and smaller drawdown in 84, 88, and 89 (each has three curves, some are difficult to distinguish). **C.** Packed-off intervals of well 88 are color-coded to match drawdown curves in D. **D.** Highly variable drawdown response times and magnitudes in intervals of 88. Response times in the observation intervals do *not* systematically decrease with increasing vertical distance of the intervals from the pumped interval in the MFZ; this behavior is an important indicator of heterogeneity.

INVERSION RESULTS: HIGHLY HETEROGENEOUS ESTIMATED 3D K

HT inversion results show an estimated K range of about 10 orders of magnitude from the high-K MFZ (10^{-1} m/s) to regions of low-K unfractured rock matrix (10^{-11} m/s). Important 3-D K features (Figure 3A) include: (1) the MFZ which varies laterally and vertically and occurs in up-dip and down-dip segments; (2) vertical low-K possible fault zone (referred to hereafter as “fault(?)”) that disrupts connectivity in the MFZ; (3) intermediate-K fractures with limited lateral extent; and (4) regions of low-K rock matrix surrounding fractures. These features identified in the 3-D K field provide a coherent explanation for heterogeneous drawdown behavior and sustained pumping rates from HT testing (superposed on K in Figures. 3B-C).

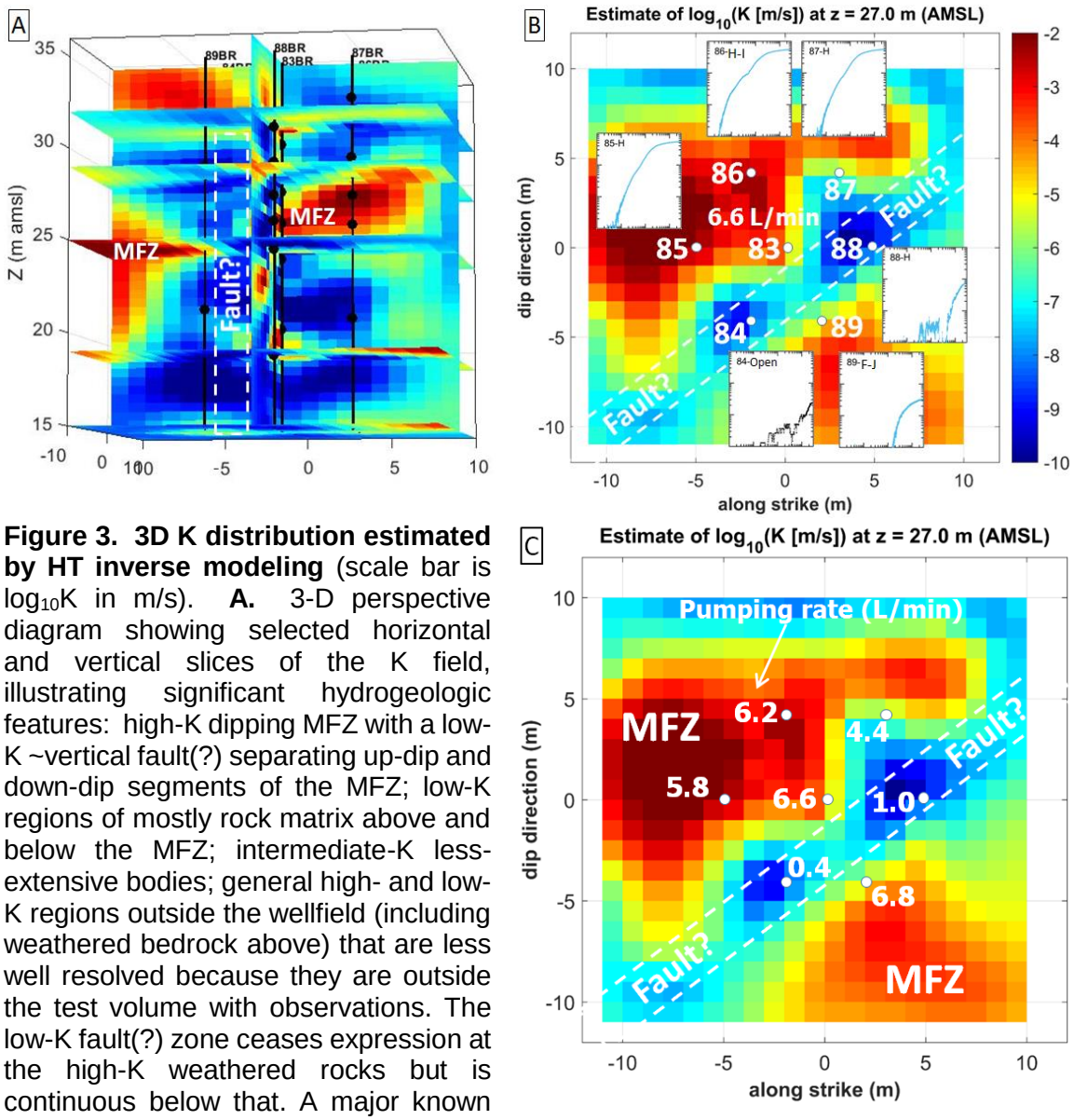

Figure 3. 3D K distribution estimated by HT inverse modeling (scale bar is $\log_{10}$K in m/s). **A.** 3-D perspective diagram showing selected horizontal and vertical slices of the K field, illustrating significant hydrogeologic features: high-K dipping MFZ with a low-K ~vertical fault(?) separating up-dip and down-dip segments of the MFZ; low-K regions of mostly rock matrix above and below the MFZ; intermediate-K less-extensive bodies; general high- and low-K regions outside the wellfield (including weathered bedrock above) that are less well resolved because they are outside the test volume with observations. The low-K fault(?) zone ceases expression at the high-K weathered rocks but is continuous below that. A major known fault is nearby at the site, has similar strike, and also is a low-K barrier to flow (Lacombe and Burton, 2010; Tiedeman et al., 2010). **B-C.** Annotated horizontal slices of K at Z = 27 m provide a map view of the low-K fault(?) separating wells 84, 88, and 89 from the up-dip segment of the MFZ containing 83, 85, 86, and 87. Pumping rates shown indicate that high rates were sustained at wells in the MFZ whereas only low rates could be sustained in the fault(?). This low-K fault(?) is consistent with the two types of hydraulic responses to tests with pumping from the MFZ at 83, 85, and 87 (Figure. 2A-B; pumping rate and responses for test in 83 are shown on Figure 3B). In particular, the fault(?) explains the hydraulic behavior of 89: i.e., delayed small responses to pumping from up-dip MFZ wells (Figures 2A-B and 3B) but high pumping rate and location in the high-K down-dip segment of the MFZ (Figure 3C).

Although the 3-D K field estimated by HT successfully identifies first-order hydrogeologic features, it is difficult to discern the geometry and connectivity of the 3-D

fracture network. In the next section, we use HT test data and K inversion results to help identify the fracture network and trace connectivity through it.

3D FRACTURE NETWORK VISUALIZATION USING DRAWDOWN SIMULATIONS

Forward modeling of the HT test in interval H of well 83 (test 83H) is used as an example for an approach to finding details of the 3-D fracture network, including connectivity, and thereby explaining complex hydrologic behavior such as is seen in Figures 2C-D. Examination of a progression of simulated drawdowns from the 83H test, along with strategic views of the K distribution, reveals hydraulic pathways and connections, or the absence thereof, between 83H and the surrounding wells (Figures 4-6).

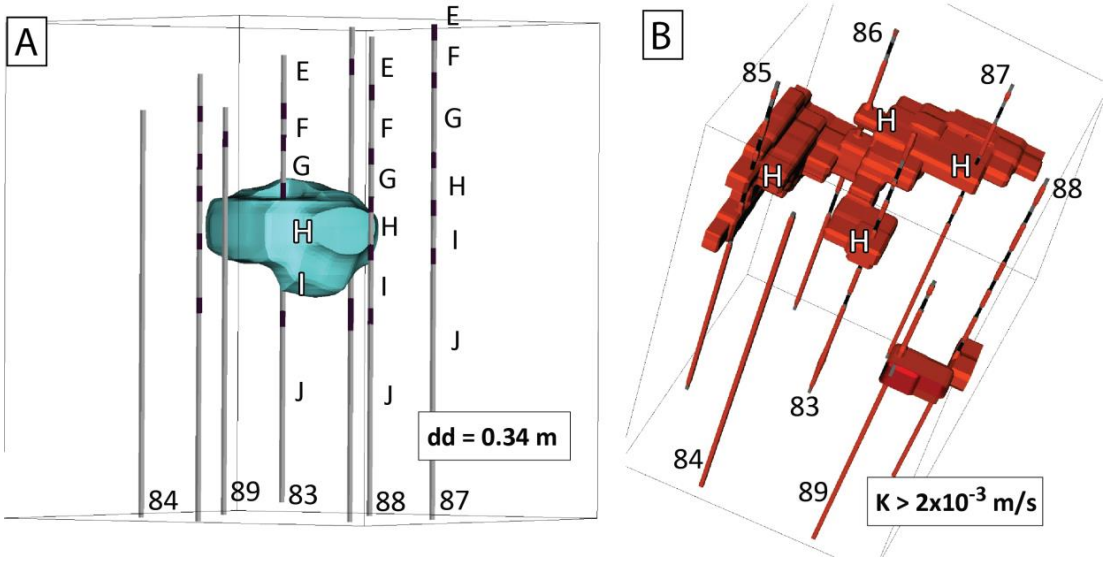

Figure 4. Simulated drawdown for test 83H, and highest-K portion of the estimated 3-D K distribution, together provide evidence of the 3-D fracture network. Letters identify packed-off intervals in 83, 88, and 87 that approximately correlate with mudstone bed stratigraphy; 87 intervals are offset upward due to up-dip elevation difference (Figure. 2A). **A.** Non-spherical isosurface of drawdown (dd) = 0.34 m at elapsed time of 120 seconds shows early indications of network structure. **B.** View from above the wellfield showing 3-D structure of estimated highest-K fractures ($K > 2\times10^{-3}$ m/s) within the MFZ. **C.** Isosurface of drawdown = 0.31 m, showing that drawdown closely follows the K structure by expanding rapidly up-dip (toward 86 and 87) through the very-high-K MFZ, but moving less rapidly toward 88, downward, and toward 84 and 89 (limited by the fault(?)). Drawdown also expands into parts of the MFZ that are lower K than shown in B (see Figure 5C), indicating how drawdown isosurfaces allow indirect visualization of the 3-D K structure because the shape of the evolving drawdown surrounds local segments of the fracture network.

Although flow is dominated by the MFZ, understanding the fracture network geometry and K distribution as a whole, including fracture connectivity that routes flow through the 3-D fracture network, is needed to design and operate in situ remediation for the volume of interest. Figure 5 shows examples of different connecting routes between the pumping zone H in well 83 and different observation zones in well 88, including multiple routes to two intervals (88F and 88J). Detailed descriptions are provided in the Figure 5 caption to assist the reader in tracing the connectivity routes.

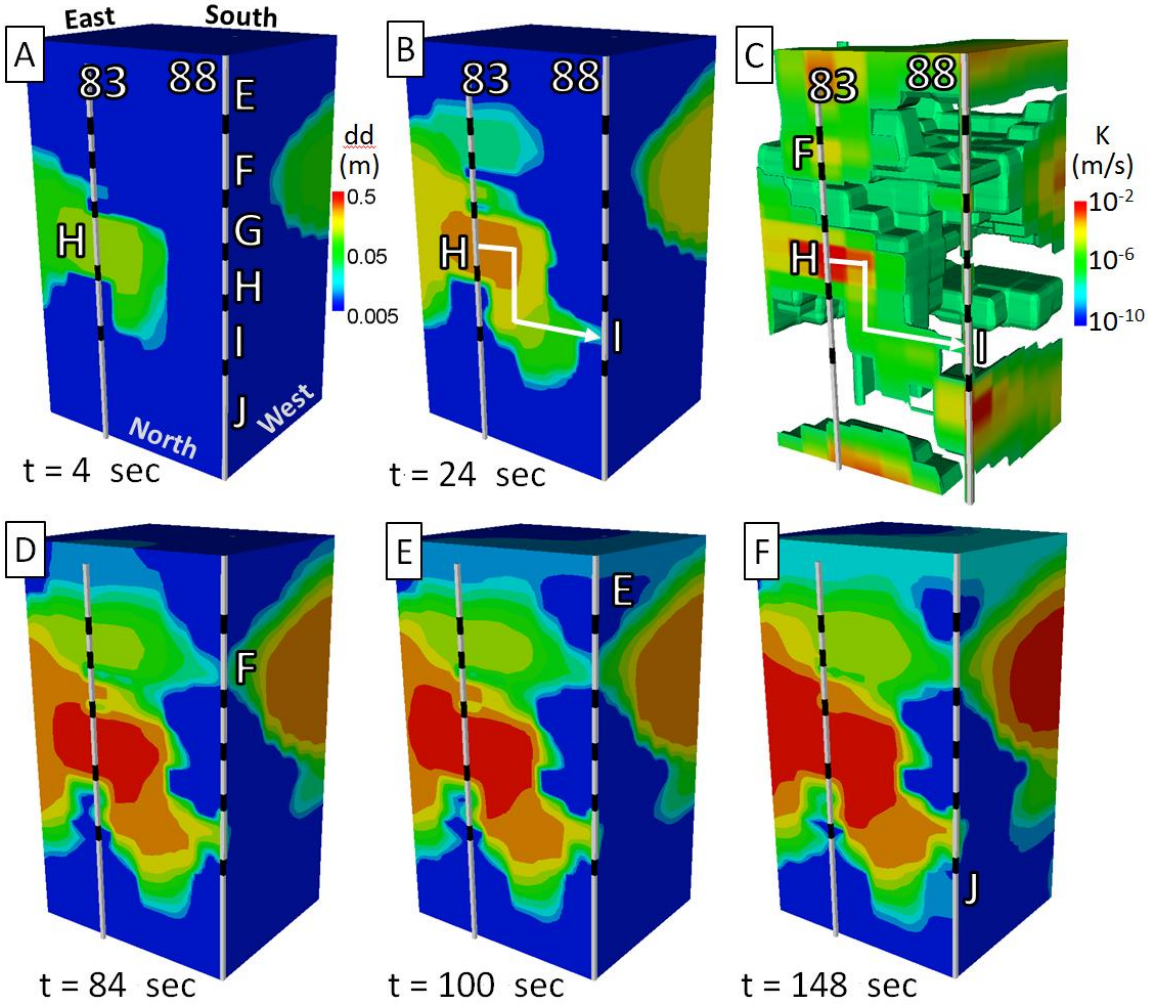

Figure 5. Network and connectivity visualization using 3-D K distribution and simulated drawdown progression from pumping at 83H to observation intervals in 88. Cropped view of 3-D wellfield volume to show a plane through wells 83 and 88 facing north and a plane through well 88 facing west (see Figure 1B and direction labels in Figure 5A). **A.** At elapsed simulated time t=4 sec since onset of pumping, drawdown moves westward and downward toward 88, and has already expanded through the MFZ towards 87 (south of 88) (see also Figures 4B-C). **B.** At t=24 sec, drawdown reaches 88 at interval I, as observed in the HT field test (Figure 2D), via branching network connections oriented generally westward (along strike) and downward (traced by white arrow). Drawdown from another connecting route via the MFZ, advances from the south (see west-facing plane) but moves slowly because of the fault(?) barrier (Figures 3B-C). Note also that a drawdown lobe associated with an intermediate-K fracture above 83H has developed. **C.** Cut-away

view through 3-D K distribution showing K values >10^{-7} m/s. Network connectivity to 88I from 83H passes through less-conductive branches traced by white arrow (compare with drawdown path in Figure. 5B). Presence of high-K MFZ is evident at 83H and south of 88 in west-facing plane (see also Figure 4C). **D.** At t=84 sec, drawdown reaches 88 in interval F (Figure 2D), initially via the network branch extending along strike through an intermediate-K fracture (shown at interval 83F in Figure 5C), and shortly afterward via the network connection from the south. **E.** At t=100 sec, drawdown reaches 88 in interval E (Figure 2D) via spreading through the regolith (Figure 1D). **F.** At t=152 sec, drawdown reaches 88 in interval J via a deeper and lower-K network branch than that connected to 88I (Figures 5B-C). In the west-facing plane, drawdown will reach 88J shortly from the south via another connectivity route.

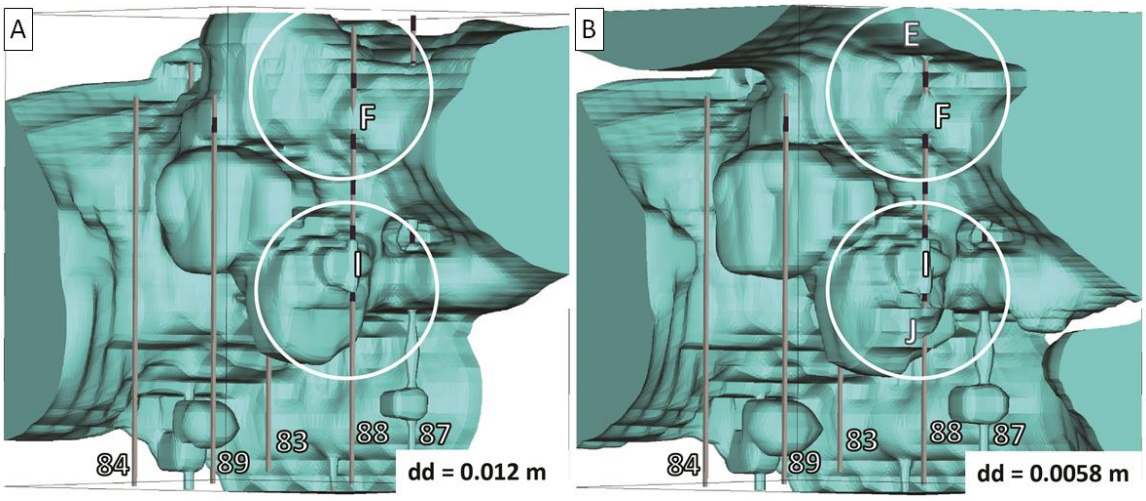

Figure 6. 3-D visualization of fracture network and connectivity using example of drawdown progression from pumping at 83H to observation intervals in 88. Isosurfaces of simulated drawdown during test 83H at elapsed time of 120 sec are used to display the 3-D details of drawdown progression within the wellfield (compare with Figures 4A and 4C showing isosurfaces of larger drawdown magnitude at the same elapsed time, which have simpler shapes in more restricted volumes). **A**. Drawdown isosurface of 0.012 m that just reaches intervals I and F in 88 (similar to drawdown reaching 88 intervals I and F in Figure 5D). **B.** Drawdown isosurface of 0.0058 m that just reaches 88 intervals E and J (similar to drawdown reaching 88 intervals E and J in Figure 5F). Circled portions of Figures 6A-B highlight the subtle differences in the expanding isosurface which can be used to trace the fracture network along which drawdown propagates. Bulbous regions surround local volumes of the aquifer influenced by local segments of the fracture network. The 3-D views of Figures 6A-B also provide evidence of the fault(?), which passes across the images in an orientation by 84 and 88 (Figure 3) but is of such low K that drawdown in it is smaller than the isosurface magnitudes. Hence the fault is conspicuous by its absence, which allows us the clear view into the 3-D volume from the viewpoint of Figures 6A-B.

Although the bulbous shapes as shown in Figure 6 may seem to obscure fracture network details within the drawdown isosurfaces and detract from the usefulness of the analysis, actually they provide valuable information that can contribute to in situ remediation design and operation. That is, drawdown volumes of influence that expand outward from segments of the fracture network help to identify those segments in two

ways: (1) fracture segments lie inside the bulbous parts of a drawdown isosurface, and (2) analysis of the incremental drawdown expansion allows recognition of incremental portions of the 3-D fracture network (see circled and other regions in Figures 6A-B). This information together with 3-D contaminant distribution data can inform strategies for "surgical" injection-withdrawal-flow control cells.

The modeling and visualization approaches presented here in Figures 4-6 are useful for recognition of the geometry and connectivity of the 3-D fracture network. However they can be time consuming and do not readily provide quantitative information such as local discharge or, in combination with concentration data, mass flux through fracture network segments of interest under different scenarios. We are currently considering other 3-D network and connectivity visualization methods that may be automated and more quantitative.

DISCUSSION AND CONCLUSIONS

HT applied to a fractured mudstone aquifer estimates the 3-D K distribution at high-resolution field scale to: (a) locate important hydrogeological features (MFZ, low-K fault(?) disrupting the MFZ, intermediate-K fractures, distribution of low-K matrix) and (b) explain heterogeneous hydraulic behavior observed in the field. Drawdown simulations using the estimated K distribution support more-detailed visualization of the 3-D fracture network, including connectivity, and locate volumes of influence around segments of the network under given test conditions.

Taken together, these capabilities of HT lead to possibilities for improved in-situ remediation design and operation, including perhaps "surgical" injection-withdrawal-flow control. To apply HT to in situ remediation, we recommend first using the 3-D K results to (a) predict tracer test behavior and (b) guide design of field tracer tests to assess the predictions, followed by tracer test modeling to estimate transport/reactivity property distributions and improve the estimated 3-D K field. These activities can then lead to more-efficient in situ remediation design and operation, supported by modeling that uses the estimated 3-D fracture network structure and connectivity, transport/reactivity properties, and contamination distribution data.

ACKNOWLEDGMENTS

This work was supported by the U.S. Geological Survey Toxic Substances Hydrology Program; National Research Program; Innovation Center; and the Advanced Research Computing group of the Core Science Analytics, Synthesis, & Libraries Program.

REFERENCES CITED

Cardiff, M., W. Barrash, and P.K. Kitanidis. 2013. "Hydraulic Conductivity Imaging from 3D Transient Hydraulic Tomography at Several Pumping/Observation Densities." *Water Resources Research,* 49(11): 7311-7326.

Hochstetler, D.L., W. Barrash, C. Leven, M. Cardiff, F. Chidichimo, and P.K. Kitanidis. 2016. "Hydraulic Tomography: Continuity and Discontinuity of High-K and Low-K Zones." *Groundwater*, 54(2) 171-185.

Lacombe, P.J. and W.C. Burton. 2010. "Hydrogeologic Framework of Fractured Sedimentary Rock, Newark Basin, New Jersey." *Groundwater Monitoring & Remediation*, 30(2): 35-45.

Leeson, A., H.F. Stroo, and P.C. Johnson. 2013. "Groundwater Remediation Today and Challenges and Opportunities for the Future." *Groundwater*, 51(2): 175-179.

NAS (National Academy of Sciences). 2015. *Characterization, Modeling, Monitoring, and Remediation of Fractured Rock*. National Academies Press, Washington DC.

Robinson, J., L. Slater, T. Johnson, A. Shapiro, C. Tiedeman, D. Ntarlagiannis, C. Johnson, F. Day-Lewis, P. Lacombe, T. Imbrigiotta, and J. Lane. “Imaging Pathways in Fractured Rock Using Three-Dimensional Electrical Resistivity Tomography.” *Groundwater*, 54(2): 186-201.

Tiedeman, C.R., P.J. Lacombe, and D.J. Goode. 2010. “Multiple Well-Shutdown Tests and Site-Scale Flow Simulation in Fractured Rocks.” *Groundwater*, 48(3): 401–415.